Available online at www.sciencedirect.com
SCIENCE DIRECT®
Journal of Sound and Vibration 281 (2005) 423–438
JOURNAL OF SOUND AND VIBRATION
www.elsevier.com/locate/jsvi

Short Communication

Effects of the chisel edge on the chatter frequency in drilling

D.N. Dilley[a,*,1], P.V. Bayly[a], A.J. Schaut[b,2]

[a]*Mechanical Engineering, Washington University, 1 Brookings Drive, St. Louis, MO 63130, USA*
[b]*Boeing Company, Advanced Manufacturing R&D, St. Louis, MO, USA*

Received 20 September 2002; accepted 21 March 2004
Available online 2 November 2004

1. Introduction

Drilling is a common metal cutting process where quality of the hole form is often a critical issue. Poor hole form is caused by tool motion during cutting; therefore, knowledge of tool vibrations is important in achieving high precision holes.

Tool dynamics was originally studied in turning and endmilling processes where time-delayed regenerative forces were responsible for instability [1,2]. Endmill stability regions found using advanced frequency domain analysis [3,4] provide combinations of axial depth of cut and spindle speed that increase metal removal rates. The use of stability lobe diagrams for milling has significantly influenced manufacturing in recent years; however, dynamic studies in drilling, reaming, and boring have been less influential. Chisel edge effects on chatter have been almost completely ignored.

Fujii et al. [5–7] showed that drill whirling created holes with odd integer hole form. The formation of odd integer lobed holes in drilling and reaming was analyzed quasi-statically by Bayly et al. [8,9]. Li et al. [10] studied the effect of rotation in boring bars, while Metzler et al. [11] estimated stability boundaries in drilling and reaming with no process damping, while Whitehead et al. [12] studied drill chatter with process damping. Rincon and Ulsoy studied the complex geometrical effects on drill vibrations [13] and the resulting forces [14].

*Corresponding author.
E-mail address: d3v@sbcglobal.net (D.N. Dilley).
[1]Currently at D3 Vibrations, 220 S. Main, Royal Oak, MI 48067, USA.
[2]Currently at Alcoa Technical Center, 100 Technical Drive, Pittsburgh, PA 15069, USA.

0022-460X/$ - see front matter
doi:10.1016/j.jsv.2004.03.065

The problem facing drilling researchers has been the complex boundary conditions of the margin and the chisel edge of the drill. Magrab and Gilsinn [15] determined buckling, frequency, and mode shape for a twisted beam with a fixed constraint and an axial force. Tekinalp and Ulsoy [16,17] created a finite element model of the drill to compare to previous experimental work. This work showed reasonable agreement to experimental structural natural frequencies; however, neither the fixed–pinned nor the fixed–fixed model was compared to chatter frequencies in drilling. Tekinalp and Ulsoy stated, "Further investigation of drill-workpiece interactions remains an important topic", yet no dynamic model including the chisel edge has since been proposed. This paper shows experimental results of the chisel point effect on the chatter frequency of the tool during drilling, and the natural frequency found in modal analysis. A simplified model, using a spring end condition to represent the chisel effects, shows improved capability over a fixed or pinned end condition.

2. Experimental methods

The source of the dominant chatter frequency is required to create a useful cutting model. The bending chatter frequency in turning and endmilling is typically found near a fixed–free tool bending frequency [1–4], whereas forced vibration produces high magnitudes at the tooth passing frequency or its harmonic. The methods for obtaining cutting data and structural data will be outlined below.

2.1. Cutting tests

Cutting tests were performed on a three-axis vertical milling machine using five different drills as shown in Fig. 1 and detailed in Table 1. The cutting tests were instrumented to collect four types of time-series data: (1) tool displacement in the fixed frame, (2) once per revolution (1/rev) signal, (3) thrust force, and/or (4) acoustic samples. This is a simplified experiment compared to a complete time, displacement, and force experiment shown in previous work [18]. Capacitance probes, a laser tachometer, a force dynamometer, and a microphone were used to collect these data as shown in Fig. 2 and Table 2.

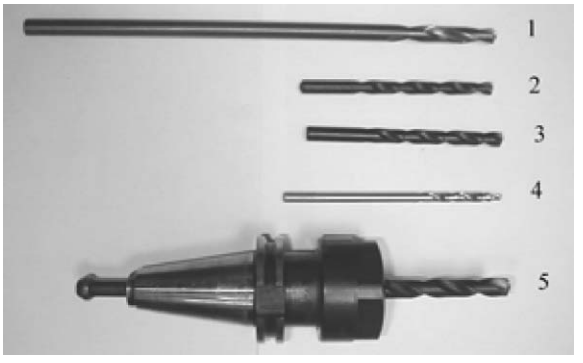

Fig. 1. Test drills.

Table 1
Twist drill geometric specifications (mm)

	Drill 1	Drill 2	Drill 3	Drill 4	Drill 5
Material	Carbide[a]	HSS M42[b]	HSS M42[b]	HSS M10[b]	HSS M42[b]
Diameter	10.72	8.73	9.53	Step drill 6.35/4.19	11.91
Web thickness	2.54	3.05	3.55	1.52	4.32
Stickout	235	97	98	107	90
Flute length	70	96	97	57/12	89

[a]Carbide: elastic modulus = 614 GPa, density = 15 000 kg/m^3.
[b]HSS: elastic modulus = 200 GPa, density = 7860 kg/m^3.

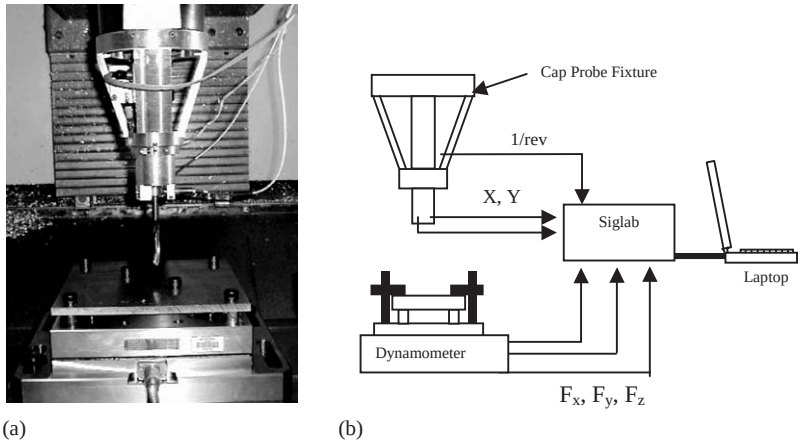

Fig. 2. Experimental setup: (a) photo, (b) schematic.

Table 2
Instrumentation

Instrumentation	Make and model
Dynamometer	Kistler 6-component force dynamometer 9255E
Capacitance probes	Lion Precision PX405HB
Data acquisition	Siglab 20-22
Laptop	IBM Thinkpad 600
Modal hammer	PCB model 086D80
Accelerometer	PCB model 309A
CNC mill	Cincinnati VMC Sabre 750
Indicator (tenth)	Starrett model 4K898
Laser tachometer	Terahertz Technologies, Inc. LT-850
Microscope/digital image	PG1000

The cutting material used was 12.7 mm thick aluminum 7050T7451B. The workpiece was mounted directly to the dynamometer for maximum part stiffness. The feed rate per revolution was 0.05 mm/tooth unless otherwise stated. The spindle speed was increased for each drill until

chatter occurred. For comparison, drilling into piloted holes was performed to eliminate the effect of the chisel edge.

2.2. Modal analysis

A standard procedure using a modal impact hammer and an accelerometer were used to determine the frequency response function (FRF). Modal analysis was performed on a non-rotating asymmetric two-flute drill, where the axes are shown in Fig. 3. Drill motion along the main cutting edge, ξ, has significant impact on the hole size and cutting force variation, while motion orthogonal to the main cutting edge, η, in the same plane has less influence on hole size and cutting forces. The two other reference frames are the space-fixed, X–Y, and another rotating frame, Ξ–H, where the modes are nearly uncoupled at the cutting edge. The uncouple direction was found where the cross FRF at the cutting edge had little response.

Hammer impacts were performed directly and crossed with the accelerometer to create a modal matrix that shows tool coupling. The accelerometer was attached as close to the end of the cutting edge as possible, where the positions are shown in Fig. 4. Roving the hammer impacts up the tool in the z-direction provided information to produce single-degree-of-freedom (1-dof) mode shapes. The torsional natural frequency was found by placing the accelerometer on one of the cutting edges, and impacting the other cutting edge. Since the torsional mode was positive direct, and the bending was negative direct, the torsional modes had opposite signs, making the mode distinguishable. Modal tests were also performed on the tool while embedded in aluminum, steel, and titanium using different preloads to investigate the effect on the tool natural frequency.

3. Experimental results

3.1. Cutting tests

The displacement and acoustic data provide information on amplitude and frequency of motion. Matlab™ software was used to estimate the power spectral density (PSD) from both the displacement and acoustic signals, in order to describe the frequency content during cutting.

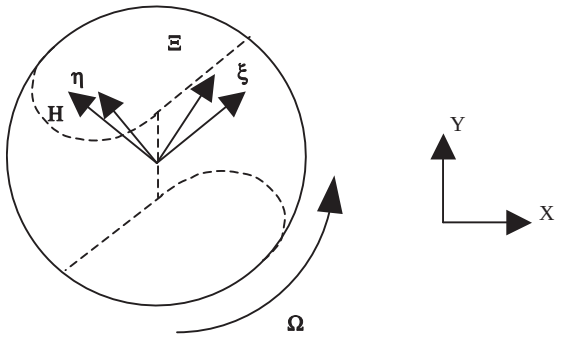

Fig. 3. Reference frames for drill motion: X–Y space-fixed; ξ–η tool-fixed, aligned with main cutting edge; Ξ–H tool-fixed, uncoupled directions.

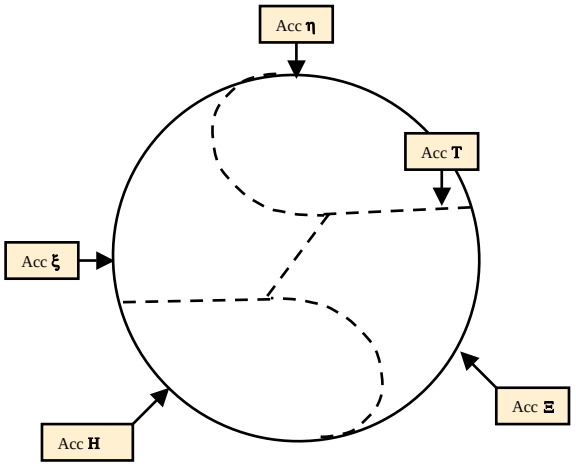

Fig. 4. Experimental modal analysis accelerometer positions, looking at drill tip. ξ is in line with drill center at cutting edge and η is orthogonal. Ξ is in direction of eigenvalue for first modeshape at cutting edge and H is orthogonal. T is the placement for torsional position.

3.1.1. Capacitance probes

A typical displacement versus time graph during unstable drilling is shown in Fig. 5. The displacement builds due to the instability, but it reaches a limit cycle of approximately 0.25 and 0.40 mm in the ξ–η frame, respectively, as measured by the capacitance probes on the drill target 100 mm from the tool tip. Fig. 5(a) shows the drilling process through a 12.7 mm plate broken into four different sections. A PSD of these time series is shown in Fig. 6(a), (c), (e) and (g) where the chatter frequency is at 566 Hz. A stable process is shown in Figs. 5(b), (d) and 6(b), (d), (f), (h) for comparison. The stable process has magnitude of amplitudes at 566 Hz that are nearly 100 times smaller than in the unstable case. Low amplitude whirling motion in the stable case is at 3 and 5 cycles/rev [5–9,12].

3.1.2. Hole profile

The onset of chatter in the unstable case occurs just before margin engagement, as shown by the frequency imprint in Fig. 7. The number of striations (cycles/rev) corresponds to the relationship between chatter frequency and spindle revolution frequency. Bayly et al. [19] found a high number of striations during torsional-axial chatter because the 1st torsional natural frequency is typically much higher than the 1st bending natural frequency. Fig. 7(a) shows the bending chatter in a hole drilled by tool 2, while Fig. 7(b) shows torsional-axial chatter in a hole drilled by tool 5. The pattern is similar in bending and torsional-axial chatter; however, the type of frequency can be distinguished by matching the striation count to the tool natural frequencies. Bending chatter is expected to be more destructive to hole quality in comparison with torsional chatter because of the effect on hole form.

3.1.3. Acoustic data

Cutting tests were performed on five tools. In four of the five tools, the bending chatter frequency is at the fixed–embedded state, while the fifth tool chattered in the torsional direction.

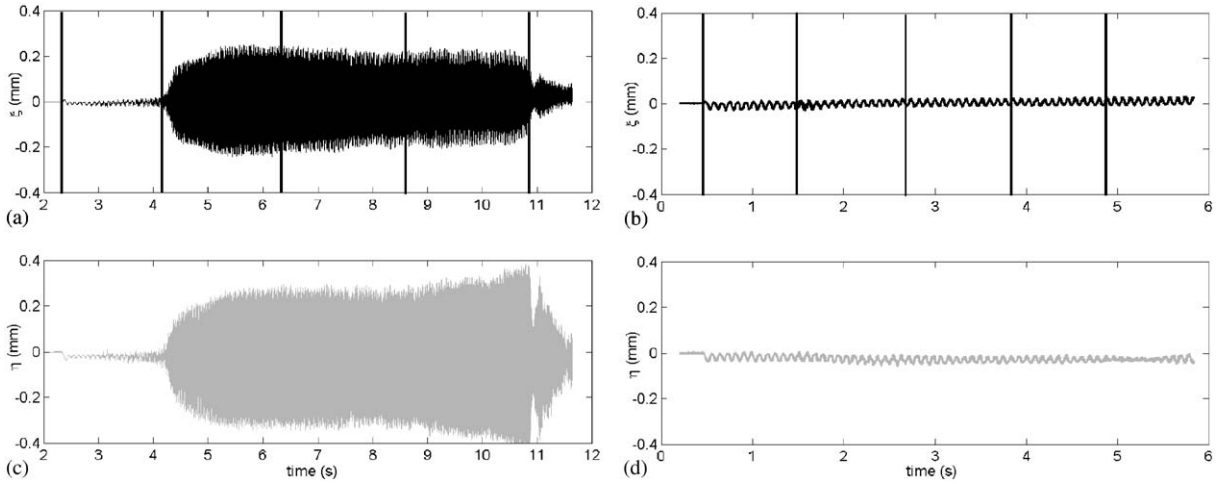

Fig. 5. Displacement versus time in tool-fixed coordinates ($\xi-\eta$) for drill 1 in aluminum 7050-T7451B at 700 rev/min; (a),(c) unstable cutting at a feed of 0.05 mm/tooth, (b),(d) stable cutting at a feed of 0.1 mm/tooth. The first section of the drilling process is prior to margin engagement, the second section is during margin engagement, and the final sections are as the drill moves gradually deeper into the workpiece with full margin engagement.

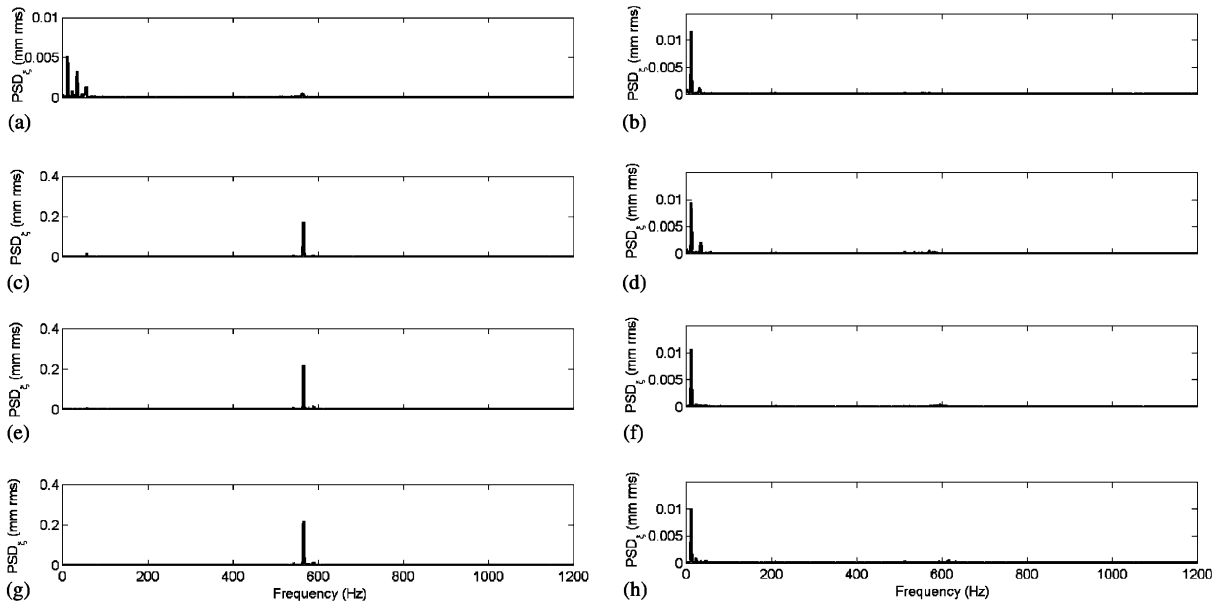

Fig. 6. PSD of displacement (ξ) time series in Fig. 5 broken into four sections noted by vertical lines in Fig. 5: (a),(c),(e) and (g) unstable at 566 Hz from Fig. 5 (a),(b),(d),(f) and (h) stable from Fig. 5(b). Frequency resolution is between 0.5–1.0 Hz depending on subfigure.

The PSD plots from the acoustic data are shown in Fig. 8 for tools 2–5, while Table 3 shows the cutting test chatter frequency. Cutting parameters leading to bending chatter were not obtained for drill 5, because torsional-axial chatter was first found in the cutting tests.

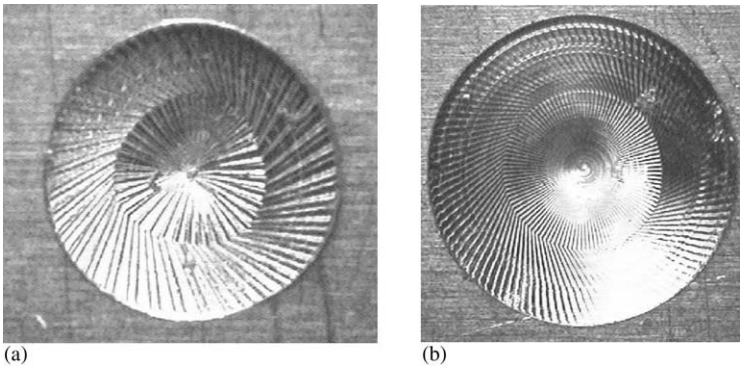

Fig. 7. Striations in the bottom of the hole caused by vibration of the drill in aluminum 7050-T7451B: (a) drill 2, 3200 rev/min, feed 0.05 mm/tooth, 2060 Hz bending chatter; (b) drill 5, 4000 rev/min, feed 0.05 mm/tooth, 7570 Hz torsional chatter.

The PSD for drill 2 cutting into a 6.35 mm pilot hole is shown in Fig. 8(e). The chatter frequency was much lower, 1180 Hz, when compared to the chatter frequency found in Fig. 8(a). This frequency is just above the bending mode of the spindle shaft. This provides evidence that the frequency shift for the fixed–embedded tool is due to the chisel edge.

3.2. Modal analysis

Past research in endmilling and turning [1–4] has shown that the bending chatter frequency is found at or slightly above the fixed–free tool bending frequency. The FRF of the fixed–free tool did not contain the 566 Hz cutting chatter frequency; therefore, extensive impact tests were performed on the tool, instrumentation, and machine structure. These test results show that the chatter frequency is related to the natural frequency of a non-rotating tool embedded into the workpiece.

3.2.1. Fixed–free

The FRFs estimated from drill 1 are shown in Fig. 9(a) where the natural frequencies are 192 and 1020 Hz for the first and second bending modes, respectively. All of the impact tests were performed at zero spindle speed where X–Y was oriented to be equivalent to ξ–η· The single-direction FRFs, $G_{\xi\xi}$, in Fig. 9(a) shows the system response in one direction, while the 2-dof system response requires a matrix of direct and cross FRFs, as in Fig. 10. A nonlinear curve-fitting procedure finds estimates of the 1st bending mode, $\omega_n = 192$ Hz, $k = 53$ N/mm, and $\zeta = 0.1\%$. There is some coupling between the ξ–η axes as shown in the off-diagonal terms of the modal matrix FRF.

3.2.2. Fixed–embedded

Results from the fixed–embedded impact test for drill 1 are shown in Fig. 9b, where the 1st and 2nd frequencies have significantly increased compared to the fixed–free mode. The matrix FRF in Fig. 11 shows coupled frequencies at 549 and 591 Hz. Perpendicular directions in which little or no

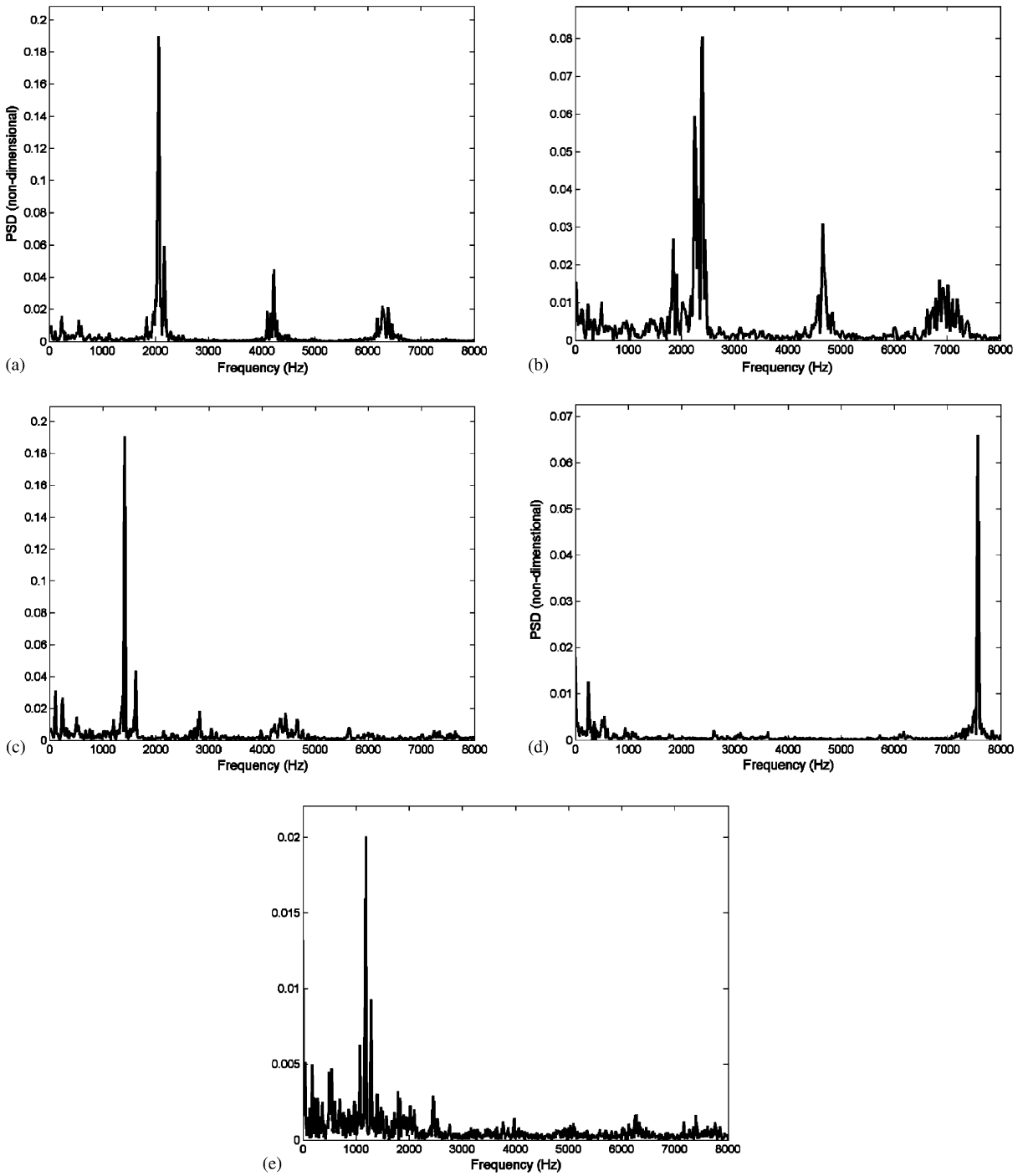

Fig. 8. PSD of acoustic sound pressure data obtained during cutting: (a) drill 2, tooth-pass frequency is 107 Hz, peak magnitude at 2060 Hz; (b) drill 3, tooth-pass frequency is 133 Hz, peak magnitude at 2390 Hz; (c) drill 4, tooth-pass frequency is 200 Hz, peak magnitude at 1400 Hz; (d) drill 5, tooth-pass frequency is 133 Hz, peak magnitude at 7570 Hz; (e) drill 2 with pilot hole, tooth-pass frequency is 107 Hz, peak magnitude at 1180 Hz.

Table 3
Cutting test results

	1	2	3	4	5
Chatter frequency (Hz)	566	2060	2390	1400	7570
Type of chatter	Bending	Bending	Bending	Bending	Torsion
Spindle speed (rev/min)	700	3200	4000	6000	4000

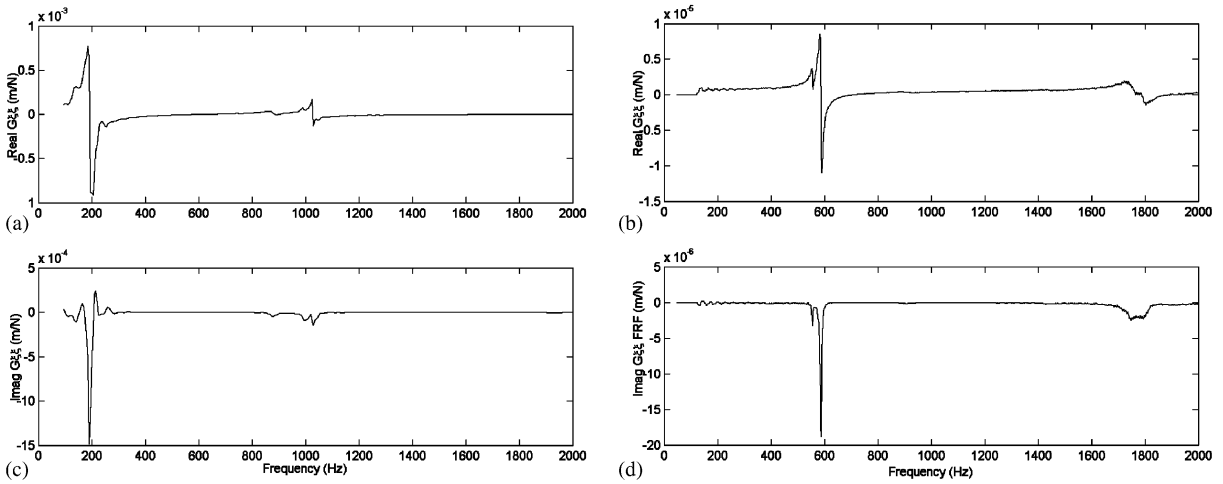

Fig. 9. Experimental displacement FRFs from tool modal tests. Shown here is the direct FRF in the tool-fixed frame: $G_{\xi\xi}(\omega)$. Results for drill 1 are shown. (a),(c) FRF of fixed–free tool; (b),(d) FRF of fixed–embedded tool.

coupling exists, Ξ–H, are shown in Fig. 12. Impact tests were performed along the z-axis of the tool with a stationary accelerometer and roving hammer to determine 1-dof mode shapes shown in Fig. 13.

Table 4 summarizes the bending frequencies for all five drills from modal analysis in the fixed–free and fixed–embedded states. The cutting chatter frequency is between the first fixed–embedded bending natural frequencies in the Ξ–H directions (Fig. 14).

3.2.3. *Material and preload effects*

Fixed–embedded modal tests were performed on the drills with different workpiece materials (aluminum, steel, titanium) and different preloads (280–850 N). The maximum naturally frequency shift was 0.2%, while the frequency resolution was 0.1% of natural frequency. This does not imply that the friction coefficient, cutting forces, or chatter limits are the same during drilling; however, the basic boundary condition that changes the natural frequency of the drill remains remarkably consistent. The natural frequency was not expected to change significantly as the dimensionless quantity $(F_z L^2)/(EI_y) << 1$; however, when this value increases, nearing buckling loads, as a result of more slender tools or increased axial forces, a more noticeable frequency shift will occur.

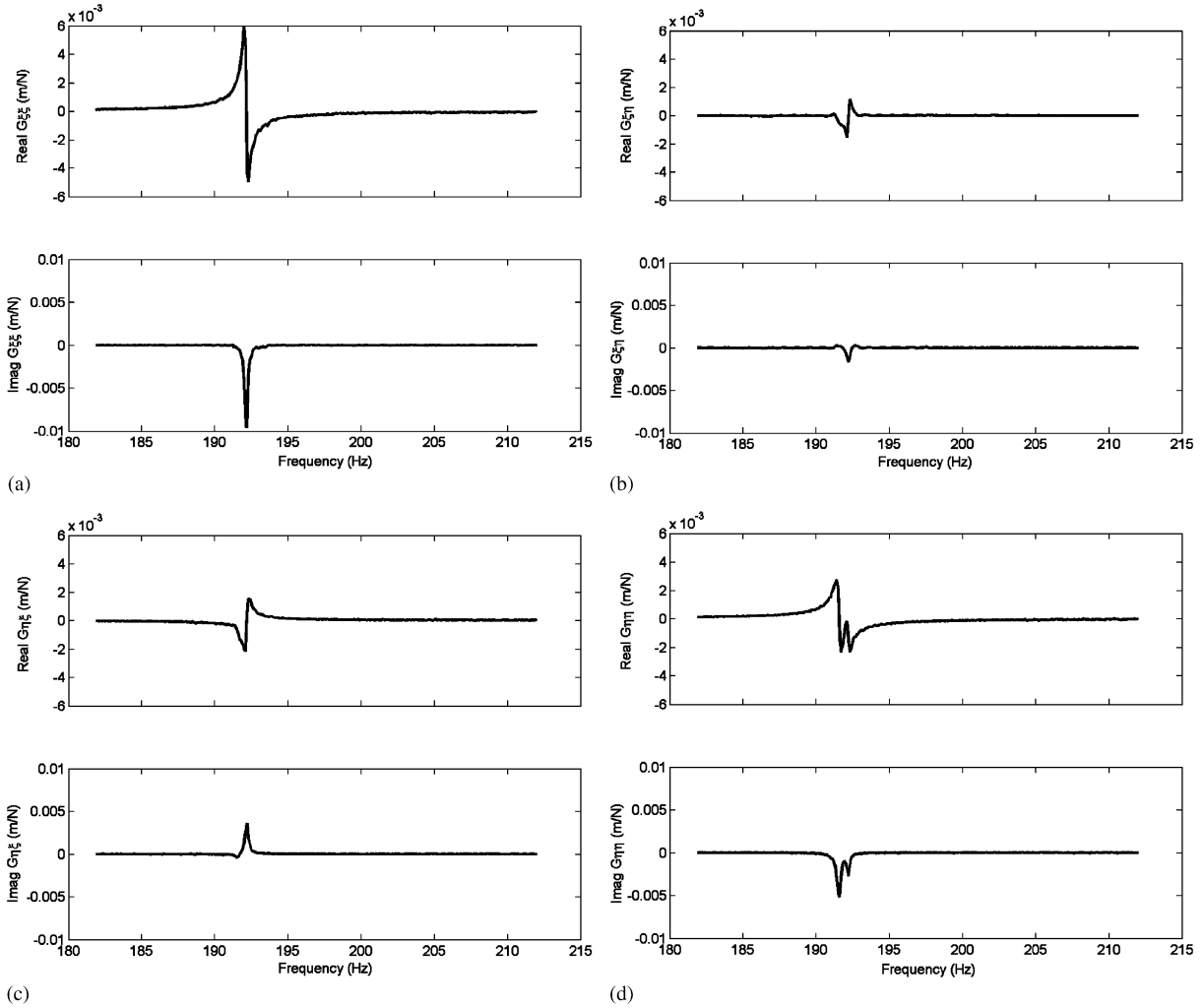

Fig. 10. Experimental displacement real and imaginary FRF matrix from tool modal tests in fixed–free condition, in the tool-fixed frame ξ–η, drill 1: (a) ξ–ξ direct, $G_{\xi\xi}(\omega)$; (b) ξ–η cross; $G_{\xi\eta}(\omega)$; (c) η–ξ cross, $G_{\eta\xi}(\omega)$; (d) η–η direct, $G_{\eta\eta}(\omega)$. Note that the diagonal terms (a),(d) represent the response in a single direction, the off-diagonal terms (b),(c) represent coupling. The linear approximation of subfigure (a) is $\omega = 192$ Hz, $k = 53000$ N/m, $\zeta = 0.1\%$. Subfigure (d) shows two frequencies at 191.5 and 192.2 Hz.

4. Analysis

A simplified 1-dof model of a drill, a long cylindrical rod, will be used to match experimental modal results. An exact solution for the frequencies and modes of a fixed–free, fixed–pinned, and fixed–fixed Euler–Bernoulli beam is available [20]. An approximate method, Rayleigh–Ritz [20,21], will be used to solve the beam equation with fixed-spring boundary conditions. The approximate method will allow for geometric changes in the structure, if desired, so the shape can

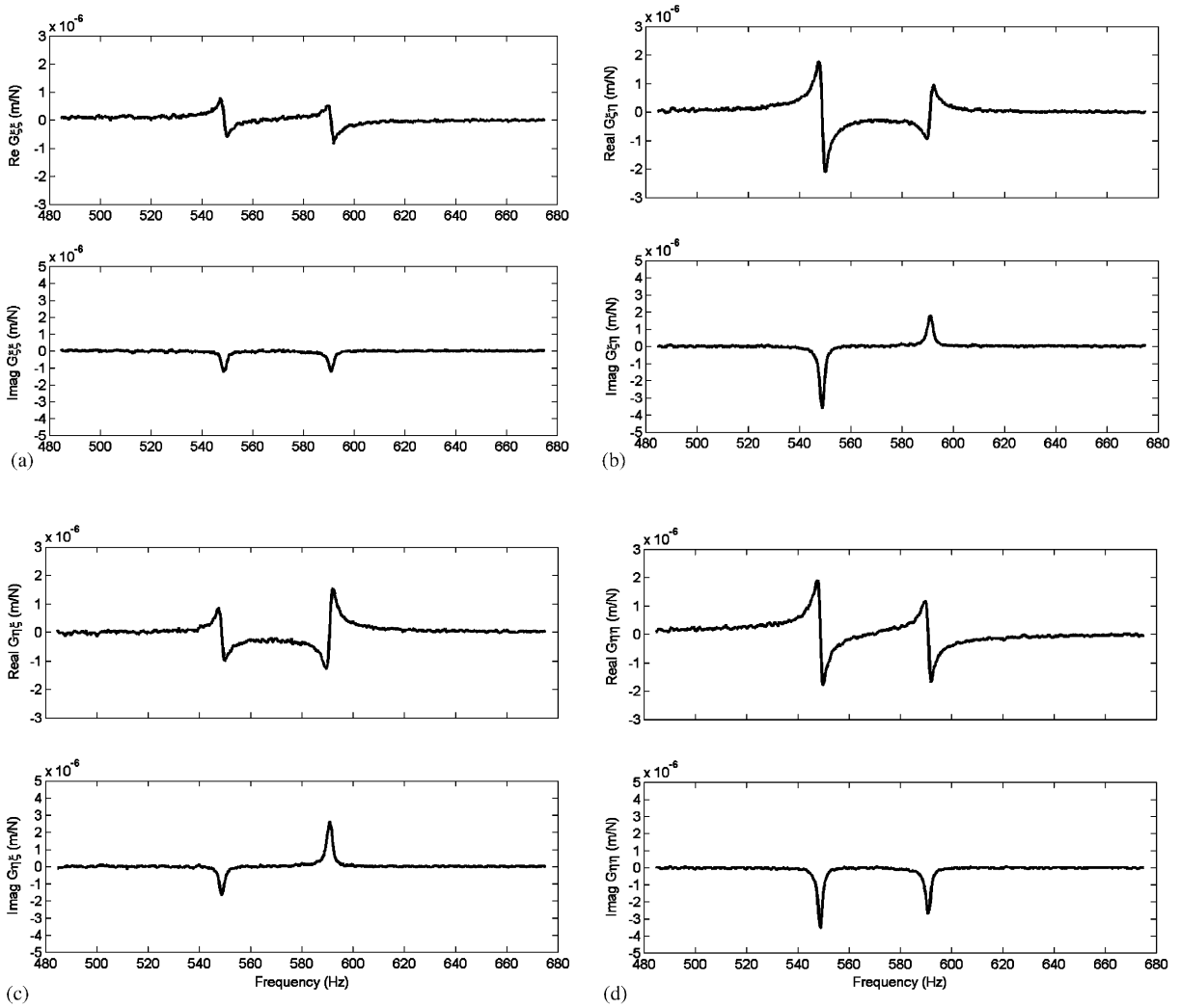

Fig. 11. Experimental displacement FRF matrix from tool modal tests in fixed–embedded condition, in the tool-fixed frame ξ–η. Results are shown for drill 1in aluminum: (a) ξ–ξ direct, $G_{\xi\xi}(\omega)$; (b) ξ–η cross; (c) η–ξ cross; $G_{\eta\xi}(\omega)$; $G_{\xi\eta}(\omega)$; (d) $\eta-\eta$ direct; $G_{\eta\eta}(\omega)$. The two peak frequencies are at 549 and 591 Hz.

be altered along the axis. Cutting force models will not be considered here, as detailed stability analysis and chatter prediction models are a topic of future work.

4.1. Derivation

The displacement in the uncoupled Ξ–H axes for a simple sdof non-rotating cylindrical beam may be assumed as a summation of trial functions ϕ and generalized coordinates q or p. The trial functions must satisfy the proper boundary conditions; therefore, the well-known frequency equation and mode shapes for the fixed–free beam are used when a spring is attached to the end of

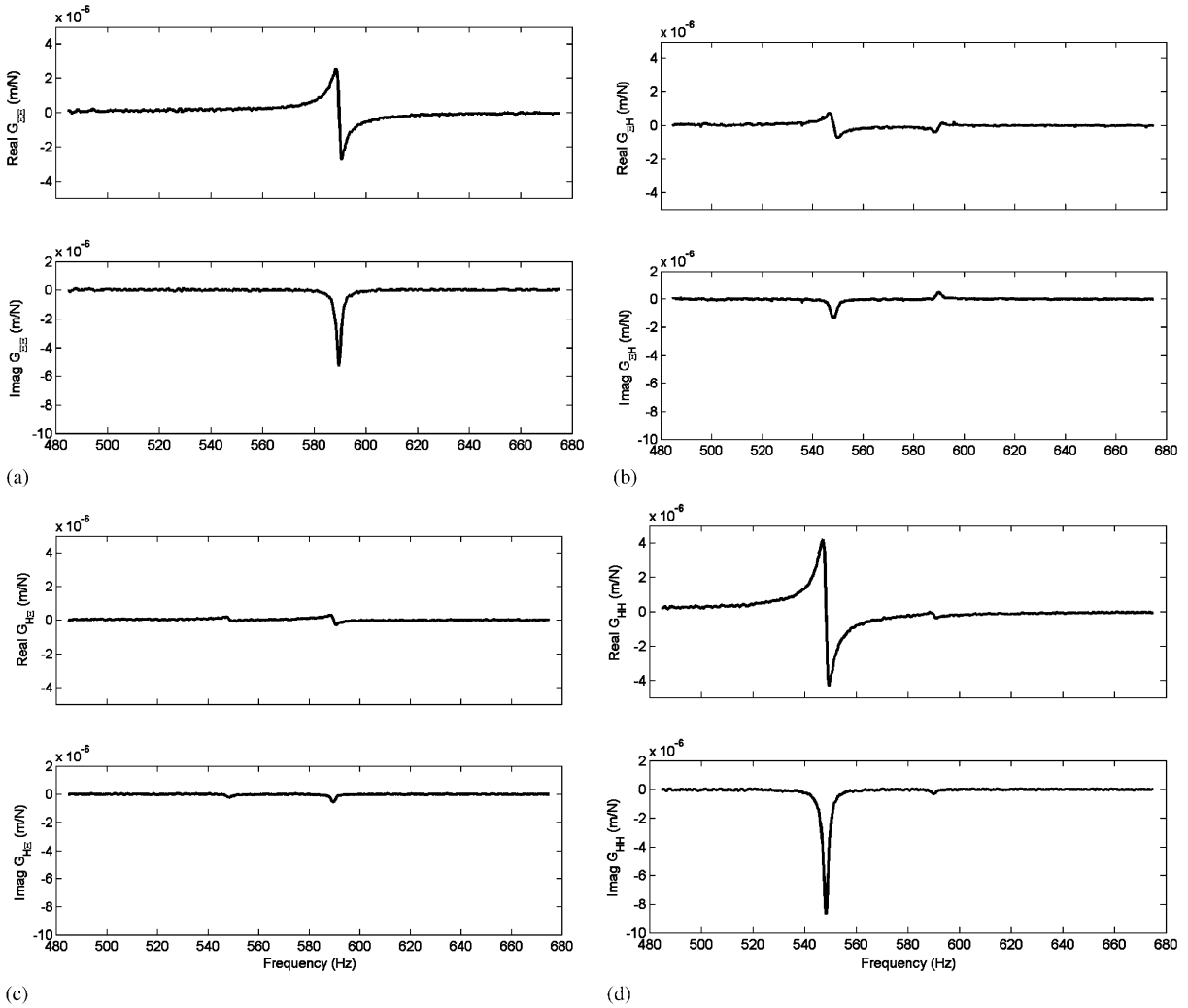

Fig. 12. Experimental displacement FRF matrix from tool modal tests in the fixed–embedded condition, in the tool-fixed uncoupled frame $\Xi-H$. Results are shown for drill 1in aluminum. (a) Ξ–Ξ direct, (b) Ξ–H cross, (c) H–Ξ cross, (d) H–H direct. The linear approximation of subfigure (a) is $\omega = 591$ Hz, $k = 4.77 \times 10^7$ N/m, $\zeta = 0.2\%$, and subfigure (d) is $\omega = 549$ Hz, $k = 2.86 \times 10^7$ N/m, $\zeta = 0.2\%$.

a fixed–free beam [20]. A transverse spring and axial thrust force are added to a simple fixed–free beam, so the equation of motion is approximated, using the Rayleigh–Ritz procedure, as

$$[m]\ddot{q}(t) + [k]q(t) = 0, \quad m_{ij} = \int_0^L \mu\phi_i(z)\phi_j(z)\mathrm{d}z, \tag{1,2}$$

$$k_{ij} = \int_0^L EI_y\phi_i''(z)\phi_j''(z)\mathrm{d}z + K_{\mathrm{end}}\phi_i(L)\phi_j(L) - \int_0^L F_z\phi_i'(z)\phi_j'(z)\mathrm{d}z. \tag{3}$$

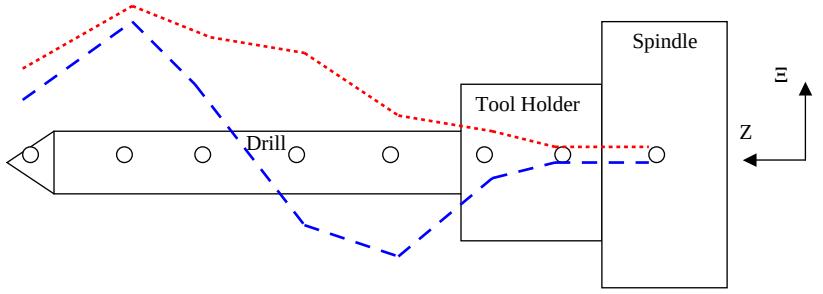

Fig. 13. First and second mode shapes of the fixed–embedded drill 1in aluminum.

Table 4
Adjusted diameter and spring stiffness for frequency correction (Ξ/H)

	1	2	3	4	5
Analytical diameter (mm)	10	7.58/8.23	9.19/9.87	5.83	11.54
Attached spring (N/mm)	955/725	4000/8100	7150/7000	570	10 500

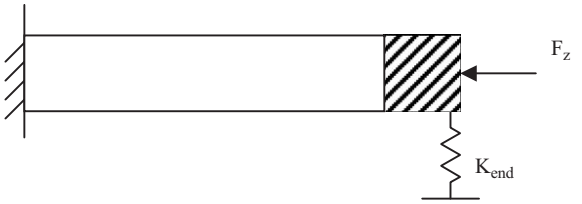

Fig. 14. Single 1-dof model of the tool. ---, first mode shape in Ξ–H direction at 549 and 591 Hz; – – –, second mode shape at 1753 and 1795 Hz.

The natural frequencies are found by solving the eigenvalue problem associated with Eq. (1). Increasing the stiffness of the attached spring will increase the frequencies, increasing the mass will decrease the frequencies, and increasing the axial preload decreases the frequencies. The definite integrals in Eqs. (2) and (3) were found numerically by integrating using 200 steps, and the first five mode shapes were used to approximate the solution.

Simply adjusting the tool diameter in the analytical model eliminates the frequency mismatch between experiment and analysis for the fixed–free condition. Also, Burnham [22] recommends modeling the fluted section of the drill by a cylindrical section approximately 78.8% of the drill diameter. In the case when a drill has different natural frequencies in the Ξ and H directions, a different diameter will be used in each direction for simplification.

The fixed–embedded tool is modeled by adding an axial preload, 640 N, and then subjecting the tip to a lateral spring force. The previous method of constraining the tip by pinning or clamping

the end [15,16] is calculated and compared to the fixed–embedded model. A fixed end condition is analogous to an infinite spring; therefore, the fixed–embedded model can never have a greater frequency than the fixed–fixed model. The following list summarizes the steps used to generate the results below: (1) determine fixed–free analytical natural frequency from measured drill geometry; (2) adjust drill diameter to match fixed–free analytical to experimental natural frequency; (3) add spring to adjusted drill to create a fixed–embedded model to match experimental natural frequency; (4) determine the analytical natural frequency by pinning the free end of (2) to compare the fixed–pinned model and fixed–embedded model.

4.2. Comparison of analysis and experiment

The natural frequency of the fixed–free drill found by experimental modal analysis is compared to the solution found from the analytical equation. Drills 2 and 3 had different frequencies in the Ξ and H directions; thus, two values are shown in Table 4. The analytical fixed–free frequencies without diameter correction are within 16% of the experimental frequencies. After adjusting the diameter of the drill, Table 5, and the fluted section, a near-exact agreement is possible. Small changes in the modeled geometry can greatly shift the frequency, where these changes include the error in the length measurement, approximation of effective flute diameter, approximation using a straight rod, and assumption that the toolholder and spindle are rigid.

Table 5 shows that the fixed–pinned solution results in errors in the range of −14.8–4.3%, which is relatively close compared to the fixed–fixed model that has errors from 50.5% to 73.8%. The drill geometry can be altered to closely match the pinned frequency; however, the fixed–free frequency is then incorrect. The attachment of springs, Table 5, to the tool tip of the fixed–free beam can provide a near-exact match to the experimental natural frequency. All of the analytical predictions were confirmed using StressCheck™ FEA software.

5. Summary and conclusions

This study shows experimental results of the effect between the chisel point and workpiece contact on the chatter frequency in non-piloted hole drilling. This chatter frequency relates to the natural frequency found using experimental modal analysis when the chisel is embedded in the workpiece.

The fixed–pinned model closely matches the experimental data; however this model does not allow the tip to move, which is shown to move during cutting. Therefore, an analytical fixed–embedded model that closely matches the frequencies found by experimental modal analysis is determined by using an appropriate spring coefficient. A more detailed model of the drill, such as the finite-element model by Tekinalp and Ulsoy [16], may provide improved results compared to the simplified drill model; however, a spring end condition should be used in either model to represent the contact between the chisel edge and workpiece, leading to improved frequency matching to experiment and quantitative stiffness results. A fixed end condition does not allow the chisel edge to have motion, which contradicts the experiments that show bending motion; therefore, using a spring boundary condition should improve future modeling efforts to understand drill motion.

Table 5
Frequencies (Hz) for 1st bending mode (Ξ/H)

	Drill 1	Drill 2	Drill 3	Drill 4	Drill 5
Experimental modal analysis fixed–free	192	466/506	554/595	442	825
Analytical fixed–free	206	540	577	481	851
	(7.3%)	(15.9%, 6.7%)	(4.2%, −3.0%)	(8.8%)	(3.2%)
Analytical fixed–free (adj.)	192	466/506	554/595	442	825
Experimental modal analysis fixed–embedded	591/549	1945/2150	2288/2400	1382	3150
Analytical fixed–pinned (adj)	542	1857/2016	2206/2369	1178	3284
	(−8.3%, −1.3%)	(−4.5%,−6.2%)	(−3.6%, −1.3%)	(−14.8%)	(4.3%)
Analytical fixed–fixed (adj.)	954	2980/3236	3540/3802	2123	5270
	(61.4%, 73.8%)	(53.2%, 50.5%)	(54.7%, 58.4%)	(53.6%)	(67.3%)

Adjusted diameter (adj.) was shown in Table 4 to match the experimental versus analytical fixed–free model. Percent error from analytical to experimental is shown.

Acknowledgments

This research was supported by the Boeing Company and the National Science Foundation Grants CMS #9625161 and DMII #9900108.

References

[1] S.A. Tobias, *Machine Tool Vibration*, Blackie and Son, London, 1965.
[2] F. Koenigsberger, J. Tlusty, *Structures of Machine Tools*, Pergamon Press, Oxford, 1970.
[3] I. Minis, R. Yanushevsky, A new theoretical approach for the prediction of machine tool chatter in milling, *Journal of Engineering for Industry* 115 (1993) 1–8.
[4] Y. Altintas, E. Budak, Analytical prediction of stability lobes in milling, *Annals of the CIRP* 44 (1) (1995) 357–362.
[5] H. Fujii, E. Marui, S. Ema, Whirling vibration in drilling. Part I: cause of vibration and role of chisel edge, *Journal of Engineering for Industry* 108 (1986) 157–162.
[6] H. Fujii, E. Marui, S. Ema, Whirling vibration in drilling. Part II: influence of drill geometries, particularly of the drill flank, on the initiation of vibration, *Journal of Engineering for Industry* 108 (1986) 163–168.
[7] H. Fujii, E. Marui, S. Ema, Whirling vibration in drilling. Part III: vibration analysis in drilling workpiece with pilot hole, *Journal of Engineering for Industry* 110 (1988) 315–321.
[8] P.V. Bayly, M.T. Lamar, S.G. Calvert, Low-frequency regenerative vibration and the formation of lobed holes in drilling, *Journal of Manufacturing Science and Engineering* 124 (2002) 275–285.
[9] P.V. Bayly, K.A. Young, S.G. Calvert, J.E. Halley, Analysis of tool oscillation and hole roundness error in quasi-static model of reaming, *Journal of Manufacturing Science and Engineering* 123 (2001) 387–396.

[10] C.J. Li, A.G. Ulsoy, W.J. Endres, The effect of tool rotation on regenerative chatter in line boring, in: R.P.S. Han, K.H. Lee, A.C.J. Luo (Eds.), *Dynamics, Acoustics and Simulations*, ASME Publication, Vol. 98, DE, 1998, pp. 235–243.
[11] S.A. Metzler, P.V. Bayly, K.A. Young, J.E. Halley, Analysis and simulation of radial chatter in drilling and reaming, *Proceedings of DETC99: 1999 ASME Design Engineering Technical Conference*, 1999.
[12] B. Whitehead, S. Calvert and P.V. Bayly, The Effect of process damping on stability and hole form in drilling, *SAE Aerofast Conference Proceedings: Aerospace Manufacturing Technology Conference & Exposition*, Seattle, WA, 2001; Paper #01AMT-35.
[13] D.M. Rincon, A.G. Ulsoy, Complex geometry, rotary inertia and gyroscopic moment effects on drill vibrations, *Journal of Sound and Vibration* 188 (1995) 701–715.
[14] D.M. Rincon, A.G. Ulsoy, Effects of drill vibration on cutting forces and torque, *Annals of the CIRP* 43 (1994) 59–62.
[15] E.B. Magrab, D.E. Gilsinn, Buckling loads and natural frequencies of drill bits and fluted cutters, *Journal of Engineering for Industry* 106 (1984) 196–204.
[16] O. Tekinalp, A.G. Ulsoy, Modeling and finite element analysis of drill bit vibrations, *Journal of Vibrations and Acoustics* 111 (1989) 148–154.
[17] O. Tekinalp, A.G. Ulsoy, Effects of geometric and process parameters on drill transverse vibrations, *Journal of Engineering for Industry* 112 (1990) 189–193.
[18] D.N. Dilley, P.V. Bayly, A.J. Schaut, Instrumentation, experimentation, and mapping techniques for vibrations in drilling, *SME NAMRC XXXI*, 2003, pp. 225–232.
[19] P.V. Bayly, S.A. Metzler, A.J. Schaut, K.A. Young. Theory of torsional chatter in twist drills, model, stability analysis, comparison to test, *Journal of Manufacturing Science and Engineering* 123 (2001) 552–561.
[20] S. Rao, *Mechanical Vibrations*, Addison-Wesley, Reading, MA, 1995.
[21] L. Meirovitch, *Elements of Vibration Analysis*, McGraw-Hill, Boston, 1986.
[22] M.W. Burnham, The mechanics of drilling small holes, *10th North American Manufacturing Research Conference*, Ontario, 1986.